ISSN 1392-1320 MATERIALS SCIENCE (MEDŽIAGOTYRA). Vol. 32, No. 4. 2026

Effect of a Zn interlayer on the Microstructure and Properties of 7075 Aluminium Alloy Resistance Spot Welding Joint

Guowei LI, Gengyuan ZHANG, Yahong LIANG *, Xinyu LIU, Yinshuang WANG, Dawei YANG, Junyan ZHU

School of Materials Science and Engineering, Inner Mongolia University of Technology, No.49, Aimin Street, Xincheng District, Hohhot, Inner Mongolia, 010051, China

http://doi.org/10.5755/j02.ms.42406

Received 30 July 2025; accepted 7 November 2025

Resistance spot welding (RSW) was carried out on a 3 mm thick 7075 aluminium alloy. A 50 μm thick Zn interlayer was added to improve the weld quality and mechanical properties of the joint. The macroscopic morphology, microstructure, precipitated phase, microhardness, and mechanical properties of the RSW joint before and after the addition of the Zn interlayer were comparatively analyzed. After adding the Zn interlayer, the microstructure and mechanical properties of the welding joints were considerably improved, and the effective range of the welding current was expanded. The grain size of the welding joint was clearly refined, the columnar crystal zone narrowed, and the equiaxed crystal zone widened. The precipitated phase changed from a reticular or long-strip-like to point- or short-strip-like and decreased in size. The number of precipitated phases increased, and the phase distribution became more uniform. The number of defects in the welding joint clearly decreased, and the joint microhardness increased. The maximum tensile shear force sustained by the Zn-RSW joint was 14.29 kN, which was 51.5 % greater than that without the Zn interlayer. The addition of the Zn interlayer changed the fracture mode from interfacial fracture to button fracture, and obvious plastic deformation occurred before the fracture. The Zn-RSW joint could absorb 245 % more energy than the RSW joint.
Keywords: resistance spot welding, aluminium alloy, Zn interlayer, microstructure, mechanical properties.

1. INTRODUCTION

Replacing traditional steel with high-strength aluminium alloys has become one of the most important measures alleviating the energy crisis and reducing environmental pollution [1, 2]. The 7075 aluminium alloy has become the primary choice for a lightweight material because of superior processing properties, good corrosion resistance, high specific strength, and low density. The 7075 aluminium alloy has been widely used in the aerospace field since the late 1940s [3 – 5]. With the progress and development of industrial technology, the 7075 aluminium alloy has also been gradually applied to automobile manufacturing. However, this alloy has a low melting point and low resistivity, and an oxide film can easily form on the surface [6 – 8]. Additionally, it is difficult to carry out welding process design and quality control of aluminium alloys [9, 10]. Therefore, achieving high-quality connections in aluminium alloys is a critical issue in the manufacturing and application fields [11, 12].

The advantages of RSW include a high production efficiency, low production cost, and easy automation. It is widely used to form connections in automobile bodies [13, 14]. However, a high welding current and electrode pressure are needed for RSW because of the high electrical and thermal conductivity of aluminium alloys [15]. Other problems include a short electrode life, spatter, and crack defects resulting from RSW of aluminium alloys [16]. Therefore, RSW joints of aluminium alloys are low-quality and have poor mechanical properties [17, 18]. Some researchers have attempted to improve these properties by adding metallic interlayers. Adding an interlayer can reduce intermetallic compound formation and serve as a bridge that closely connects two metals [19].

Chen et al. [20] studied the effect of adding a Zn interlayer to a RSW joint of DP600 steel and an A5052 aluminium alloy. The addition of Zn affected the growth morphology of the intermetallic compounds. Compared with the RSW joint without the interlayer, the RSW joint with a Zn interlayer could sustain a 28% higher tensile shear force and was considerably more plastic. Bryan et al. [21] used a stainless steel interlayer to perform RSW of dissimilar metals. The stainless steel interlayer prevented the formation of Fe–Al intermetallic compounds and increased the tensile shear force that could be sustained by the joint by 4.8 kN. Zhang et al. [22] studied the influence of an Al/Zn interlayer on the properties of RSW joints of a Mg–Al alloy. After Al addition, cracks in the sample became discontinuous, whereas Zn addition eliminated cracks in the sample. Crack suppression improved the mechanical properties of the sample. Liu et al. [23] reported that the inclusion of a Nb interlayer affected the properties of RSW joints of titanium and steel. The addition of Nb improved the microstructure of the welding joint. Using a welding current of 7 kA produced a joint that could sustain a tensile shear force of 4.3 kN. Qin et al. [24] studied the influence of an Al–Si interlayer on the microstructure and properties of RSW joints of Al–Mg_2Si–Si. The addition of the Al–Si interlayer considerably increased the nugget diameter, reduced the energy consumed during welding, and increased the tensile shear force sustained by the joints.

* Corresponding author: Y. Liang
E-mail: *liangyahong@imut.edu.cn*

In summary, the addition of suitable interlayer materials can considerably improve the microstructure and properties of RSW joints. Adding an interlayer reduces the formation of intermetallic compounds, promotes metallurgical bonding between dissimilar metals and reduces the number of defects and energy consumption during welding. Many studies have been carried out on using interlayers to enhance the microstructures and mechanical properties of RSW joints of dissimilar metals, but only a few have focused on RSW of a single metal. Therefore, the objective of this study was to use a Zn interlayer to increase the weld quality of RSW joints of 7075 aluminium alloy. The microstructures and mechanical properties of the joints before and after the addition of the welding Zn interlayer were analyzed. This analysis provides necessary reference data and theoretical support for improving the quality and properties of RSW joints of 7075 aluminium alloy with a Zn interlayer.

2. MATERIALS AND METHODS

The material investigated in this study was a 3 mm thick AA7075 aluminium alloy with cutting dimensions of 70 mm × 25 mm, and a 50 μm thick Zn interlayer with cutting dimensions of 25 mm × 25 mm. RSW was performed using a DN-200 medium-frequency direct current welding machine. Cr–Zr–Cu was used as the welding electrode material with an end diameter of 8 mm. The welding current was increased from 27 kA to 33 kA in 1 kA increments, the welding time was 400 ms, and the electrode pressure was 5.5 kN. Fig. 1 is a schematic of the RSW process.

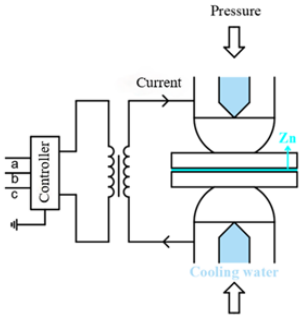


Fig. 1. Schematic of the RSW process

Tests on the microstructure and mechanical properties of the welding joints were carried out in accordance with the AWS D8.2M:2017 standard [25]. An INSTRON 5982 universal testing machine was used to measure the tensile shear force. As shown in Fig. 2, 3 mm thick pads were placed at two ends of the sample, and the tension speed was set at 1 mm/min.

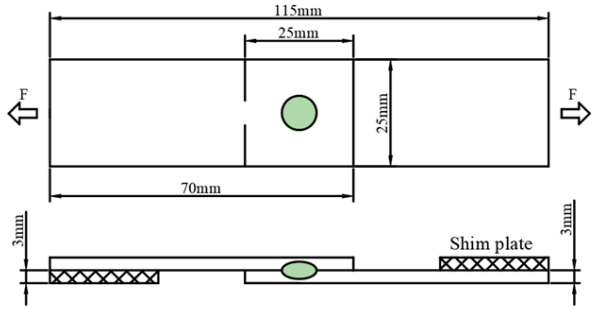


Fig. 2. Schematic of the tensile shear test

The macroscopic morphology of the welding joint was observed via a STEMI 2000-C stereomicroscope. The microstructure was observed via a metallographic microscope. The microhardness of the welding joints was measured with an FM-810 microhardness tester. The tester parameters included a dwell time of 15 s, a force of 2 N, and a measurement distance of 0.2 mm. An FEI Quanta 650 FEG field emission environmental scanning electron microscope (SEM) was used to observe the microstructure of the welding joint and to measure electron back-scattered diffraction (EBSD) patterns. After mechanically grinding, the samples were electrochemically polished using a DC-regulated power supply, with a solution of 90 % ethanol and 10 % perchloric acid serving as the electrolyte. The polishing time was 70 to 90 s, and the polishing voltage was 30 V. The EBSD operated at 20 kV high voltage and 2.25 m step length. The distribution of alloying elements was determined via energy dispersive spectroscopy (EDS). The phase composition was analyzed via X-ray diffraction (XRD). The test parameters included a step size of 0.02°, a scan speed of 5°·min^{-1}, and a scan range of 10° to 90°.

3. RESULTS AND DISCUSSION

3.1. Tensile shear force and nugget diameter

The tensile shear force and nugget diameter of RSW joints of 7075 aluminum alloy with a Zn interlayer are shown in Fig. 3 and Fig. 4, respectively.

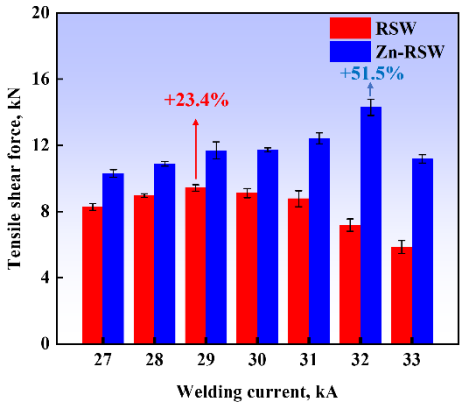


Fig. 3. Tensile shear force of the RSW and Zn-RSW joints

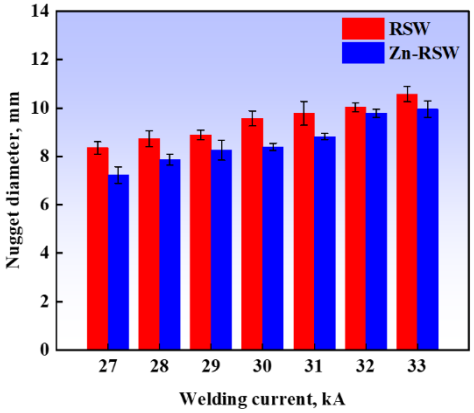


Fig. 4. Nugget diameter of the RSW and Zn-RSW joints

Fig. 3 shows that with increasing welding current, the tensile shear force sustained by the welding joint (both

before and after adding the Zn interlayer) increased and then decreased. When the welding current was 29 kA, the RSW joint reached a peak of 9.43 kN. After adding the interlayer Zn, the Zn-RSW joint tensile shear force was greater than the RSW joint tensile shear force at the same welding current. At a welding current of 29 kA, the Zn-RSW joint sustained a tensile shear force of 11.69 kN, which was 23.4 % greater than that for the RSW sample. As the welding current increased, the tensile shear force sustained by the Zn-RSW joint peaked at 14.29 kN, which was 51.5 % greater than that for the RSW joint.

At the same welding current, the RSW joint had a larger nugget diameter than the Zn-RSW joint, as shown in Fig. 4. The nugget diameter of the RSW and Zn-RSW joints gradually increased with the welding current. Bijoy et al. [26] reported that increasing the nugget diameter can considerably improve the bearing capacity of a joint. However, a large nugget diameter results in increasing spatter of the welding joint and defects are easily generated inside the nugget. Therefore, the mechanical properties of the joints began to decrease with increasing nugget diameter. Interfacial fracture occurred in the RSW joint at the optimal welding current of 29 kA, whereas button fracture occurred in the Zn-RSW joint at an optimal welding current of 32 kA.

The addition of the Zn interlayer not only increased the joint tensile shear force but also expanded the effective range of the welding current. According to AWS D8.2 M:2017 [25], the minimum use requirement of the welding joint in this test is a nugget diameter of 7 mm and a minimum welding joint tensile shear force of 9.1 kN. According to Fig. 3 and Fig. 4, under the premise that the nugget diameter and tensile shear force meet the standard, the effective range of the RSW welding current was 29 kA – 30 kA for the RSW joint and 27 kA – 33 kA for the Zn-RSW joint. In the absence of an interlayer, the minimum welding current that met the use requirements was 29 kA. Addition of the Zn interlayer reduced the minimum welding current to 27 kA. Therefore, adding a Zn interlayer can also reduce the energy consumption of the welding process. This will help manufacturers save energy and reduce costs.

3.2. Microstructure and EDS analysis

Fig. 5 shows the cross-sectional morphologies of the welding joints before and after the addition of the Zn interlayer. With increasing welding current, the nugget diameter of the RSW and Zn-RSW joints gradually increases. As the welding current is 29 kA, there are no discernible shrinkage cavities or crack defects in the nugget. Fig. 5 b shows that when the welding current reaches 32 kA, large shrinkage cavities and cracks appear inside the RSW joint. Fig. 5 d clearly shows that the shrinkage defects disappear after the addition of the Zn interlayer.

Fig. 6 shows the microstructures of the RSW and Zn-RSW joints. In both cases, four zones were observed in the welding joints: the base metal, a heat-affected zone, a columnar dendrite zone, and an equiaxed crystal zone. Fig. 7 shows EBSD maps of the joints. Fig. 7 a corresponds to the A region of Fig. 5 a, Fig. 7 b corresponds to the B region of Fig. 5 b, and Fig. 7 c corresponds to the C region of Fig. 5 d, and the directions are rotated clockwise by 90°.

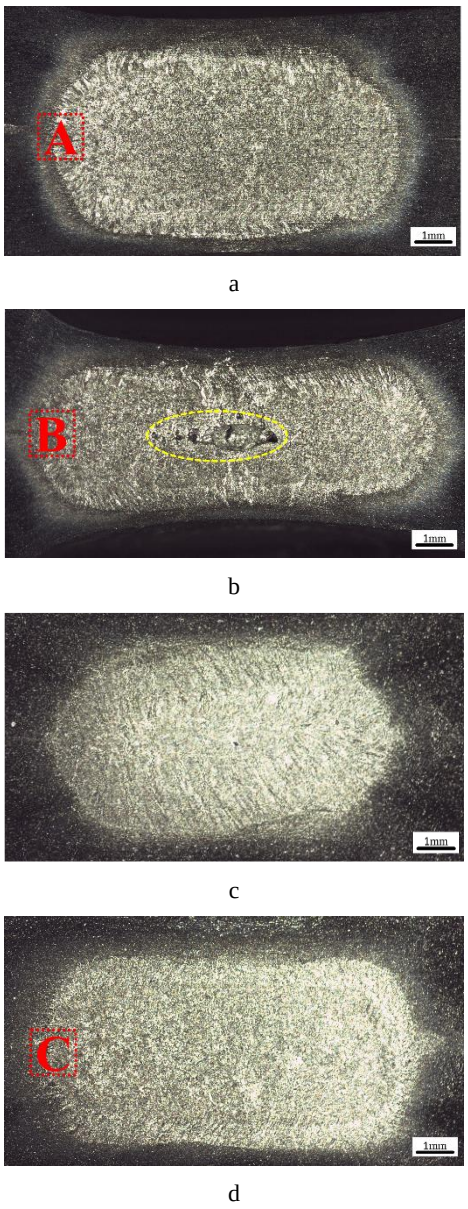


Fig. 5. Cross-sections: a – RSW joints at 29 kA; b – RSW joint at 32 kA; c – Zn-RSW joints at 29 kA; d – Zn-RSW joints at 32 kA

In Fig. 7, the width of the columnar crystal zone of the 32 kA RSW joint is the largest, which is due to the increase of heat input with the increase of welding current. In addition, the columnar crystal zone is clearly narrower for the Zn-RSW joint than for the 29 kA RSW joint. The width of the columnar crystal zone is approximately 330 μm for the 29 kA RSW joint and 150 μm for the Zn-RSW joint. The columnar crystals in the Zn-RSW joint are also smaller than those in the RSW joint. This result is obtained because as the welding current increases, the heat input to the Zn-RSW joint increases, but increasing the elemental Zn content reduces the solidus temperature of the alloy, causing the melt to overheat. Generally, the degree of supercooling of the melt increases with the melt superheating, which increases the nucleation rate. With increasing nucleation rate, both the number of nuclei in the liquid phase and the number of newly formed grains increase. The newly formed grains are in contact with the columnar crystals, which further limits crystal growth [27, 28].

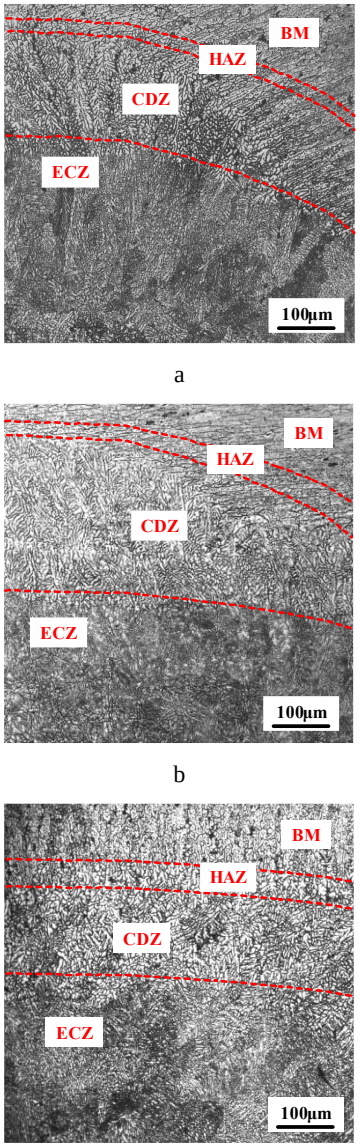


Fig. 6. Microstructure of the joints: a – no interlayer, 29 kA; b – no interlayer, 32 kA; c – Zn interlayer, 32 kA

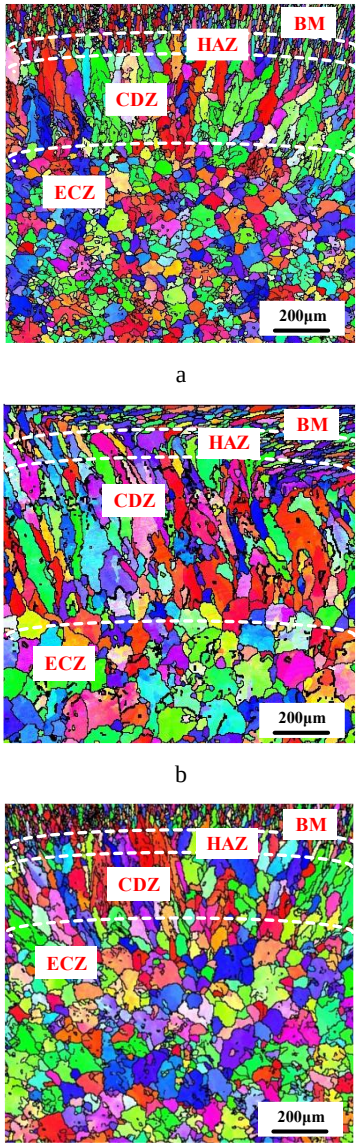


Fig. 7. EBSD maps of the joints: a – no interlayer, 29 kA; b – no interlayer, 32 kA; c – Zn interlayer, 32 kA

Fig. 8 shows the grain orientation distribution of the equiaxed grain zone in the nugget center, and Fig. 9 shows the equiaxed grain zone's average grain size. Fig. 8 and Fig. 9 show that, in the absence of an interlayer, with the welding current increasing, the RSW joint heat input increases, and the grain size gradually increases. At a welding current of 29 kA, the average grain size is 22.5 μm. As the welding current increases to 32 kA, the average grain size increases to 32.9 μm, which is 46.2 % greater than that at 29 kA. An increase in the grain size reduces the deformation ability of the alloy, resulting in poor plasticity. Moreover, an excessive number of grains results in differences in the strengths of grain boundaries, induces cracks, and reduces the alloy toughness. At a welding current is 32 kA, the addition of the Zn interlayer considerably reduces the grain size of the welding joint. The average grain size is 32.9 μm in the joint without the interlayer and 25.4 μm in the joint with the interlayer, corresponding to a reduction of 29.5 %, which manifests as grain refinement.

Grain refinement can be explained by the different heat generated during RSW. The heat generated is determined by Joule 's law.

$$Q = I^2Rt(J). \quad (1)$$

The heat input by resistance spot welding is affected mainly by the welding current I (A), the electrode resistance R (Ω) and the welding time t (s). As the welding current and welding time remain unchanged, the electrode resistance is proportional to the welding heat input. The resistance between the electrodes includes the resistance *Rw* of the workpiece itself, the contact resistance *Rc* between the two workpieces, and the contact resistance *Rew* between the electrode and the workpiece, as shown in Fig. 10 a.

$$R = 2Rw + Rc + 2Rew. \quad (2)$$

At the beginning of resistance spot welding, the uneven surface of the base metal prevents complete contact between the two workpieces upon lap placement.

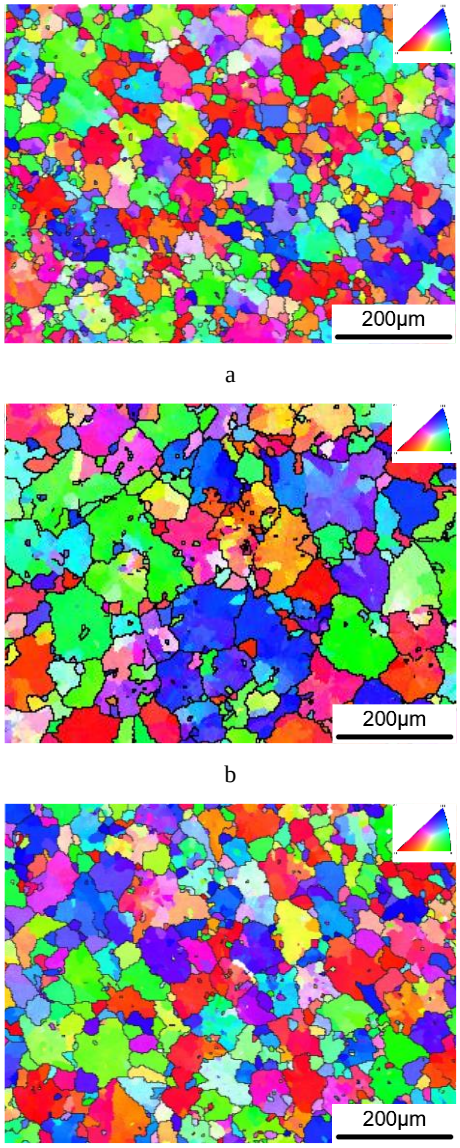


Fig. 8. Grain orientation in the ECZ of the nugget center: a – no interlayer, 29 kA; b – no interlayer, 32 kA; c – Zn interlayer, 32 kA

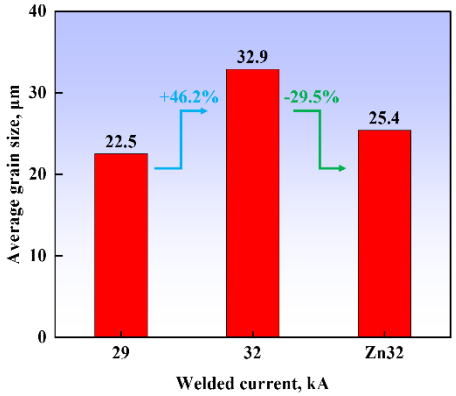


Fig. 9. Average grain size of the ECZ

Pressurization deforms the contact point between the two workpieces, which increases the contact area between the plates, as shown in Fig. 10 a.The thin soft added Zn interlayer causes the contact area between the plates to increase with the pressure.

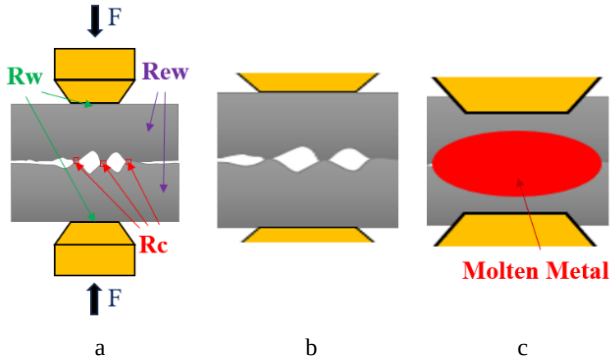


Fig. 10. Schematic of the welding process of a joint without an interlayer: a – before welding; b – in the welding process; c – the nugget morphology after welding

The current through the narrow interfacial area decreases, reducing the contact resistance and thereby, the welding heat input, as shown in Fig. 11 a.

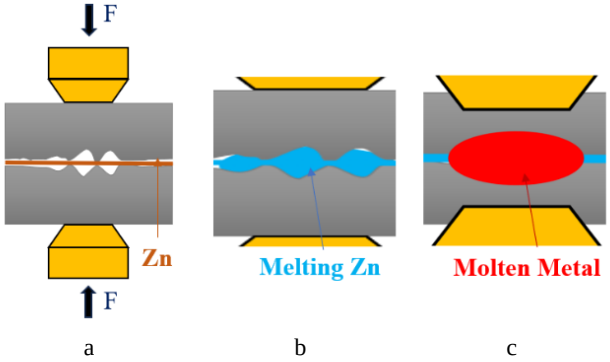


Fig. 11. Schematic of the welding process of a joint with an added Zn interlayer: a – before welding; b – in the welding process; c - the nugget morphology after welding

During welding, the melting point of Zn is lower than that of the base metal, causing the Zn interlayer to melt preferentially and fill the gap between the plates, which increases the contact area and thereby reduces the contact resistance and the heat input, as seen in Fig. 11 b. The decrease in the heat input causes the nugget diameter to decrease, as shown in Fig. 10 c and Fig. 11 c. Compared with the results for the joint without the interlayer, the decrease in the heat input to the joint with the Zn interlayer results in a relatively small nugget diameter and decreases the grain size, manifesting as grain refinement.

Furthermore, the addition of the Zn interlayer makes up for the burning loss of the Zn element caused by the welding process. During welding, mutual diffusion occurs between Al and Zn. During the cooling process, due to the extremely low solubility of Zn in Al at low temperature, a fine two-phase microstructure is finally formed, including an α-Al phase and Zn-rich phase particles. These fine second phase particles can pin grain boundaries, effectively hinder grain growth, and strengthen the joint through the second phase strengthening mechanism [29, 30]. According to the study of Li et al. [31], grain refinement can reduce stress concentration and enhance deformation uniformity [32, 33]. Therefore, grain refinement can improve the strength and

hardness as well as the plasticity and toughness of welding joints.

Fig. 12 shows a BSE image of the nugget zone. Fig. 12 a and Fig. 12 b shows a large precipitated phase in the joint without an interlayer, grains distributed along the crystal boundary in a reticular or long strip, and shrinkage defects in the nugget.

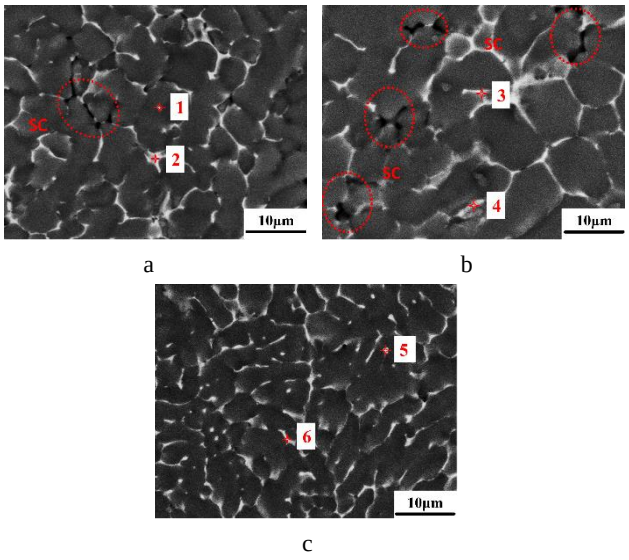


Fig. 12. BSE images of the nugget center before and after the addition of the interlayer: a – no interlayer, 29 kA; b – no interlayer, 32 kA; c – Zn interlayer, 32 kA

The action of tensile stress results in a high stress concentration in the shrinkage cavity, and a crack source is preferentially generated. The crack easily expands along the coarse precipitated phase, resulting in intergranular brittle fracture [34]. As the welding current increases, the size of the precipitated phase increases and the number decreases. In addition, the size and number of shrinkage cavities increase. As shown in Fig. 12 c, the addition of the Zn interlayer reduces the size of precipitated phases and increases their number, and low number of shrinkage cavities. The phase distribution becomes more uniform, with a point-like or short-strip distribution at the grain boundary, consistent with the study of Li et al. [35]. The number of shrinkage defects is considerably reduced, which can improve the mechanical properties of the welding joint [36]. When subjected to impact or vibration, this fine uniform precipitated phase can absorb a large quantity of energy. The defect-free joint has no prominent stress concentration, which prevents cracking of the joint.

The precipitated phases of different shapes in Fig. 12 were analyzed by EDS point scanning, and the results are shown in Table 1.

Table 1. Analysis of the chemical composition at the EDS points of the characteristic phases

Spectrum	Element, atomic %			
	Mg	Zn	Al	Cu
1	3.76	3.52	91.79	0.93
2	8.26	6.23	82.26	3.25
3	1.90	4.81	91.97	1.32
4	2.08	3.93	92.93	1.06
5	5.27	5.94	85.43	3.36
6	6.69	6.60	84.98	1.73

According to it, the components of the precipitated phases in the nugget zone before and after the addition of the interlayer are Mg, Zn, Al, and Cu. The nugget zone was analyzed by XRD, and the results are shown in Fig. 13.

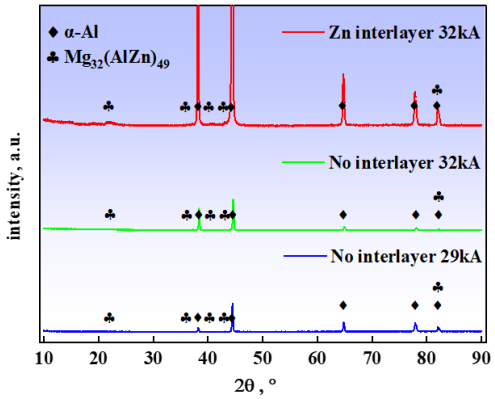


Fig. 13. XRD patterns for the nugget zone

Compared with the XRD pattern of the RSW joint, the diffraction peaks in the XRD pattern obtained after addition of the interlayer are located at essentially the same positions and are stronger. The nugget zone is composed of α-Al and $Mg_{32}(AlZn)_{49}$ (T phase). Addition of the Zn interlayer changes the size and number of precipitated phases in the nugget, but it does not change the type of precipitates.

3.3. Microhardness

Fig. 14 shows the welding joint microhardness distribution before and after adding the Zn interlayer. The nugget zone is a weak area of microhardness, and the hardness value is about 70 % of the base metal. In the case of no interlayer, the average microhardness of the nugget center is 113.2 HV when the welding current is 29 kA, and the average microhardness is reduced to 105.8 HV when the welding current is 32 kA. With increasing welding current, the microhardness gradually decreases.

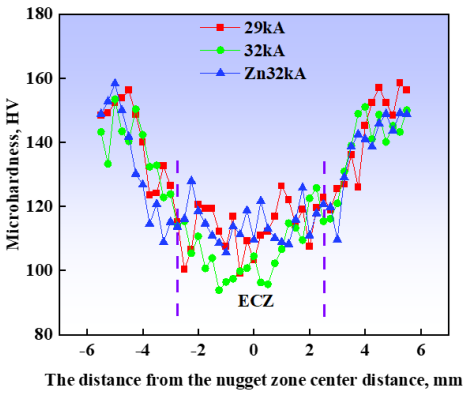


Fig. 14. Microhardness distributions of the welding joints

This result is obtained because the heat input increases with the welding current, which increases the volume of molten metal in the welding joint. The expansion speed of the plastic ring cannot keep pace with the melting speed of the aluminum alloy, causing the liquid metal to break through the plastic ring boundary, resulting in surface and internal splashing. As a result, there is insufficient liquid metal inside the nugget, and shrinkage cavities and crack

defects form during solidification shrinkage. As a result of the presence of defects, the internal nugget structure is not dense. Second, the increase in the heat input increases the grain size [37, 38]. The presence of defects and large grains causes the microhardness of the welding joint to fluctuate greatly, resulting in a low hardness.

At a welding current of 32 kA, the average microhardness of the weld with the added Zn interlayer is 114.4 HV, an increase of 8.1 % from that without the interlayer (105.8 HV). The microhardness test reveals that after the interlayer was added, a fine-grain zone forms in the nugget. The microhardness of the fine-grain zone is 128 HV, which is considerably greater than that of the other regions, reaching 86.5 % that of the base metal. This result is obtained because after entering the weld, the liquid interlayer metal becomes more fluid, the size of the shrinkage cavity and number of crack defects are considerably reduced, and the nugget density increases. At the same time, the sizes of the grains and precipitate phase in the joint are refined and the areas of the grain boundaries and phase boundaries are increased, which can hinder dislocation motion and crack expansion. The uniform distribution of the fine and dispersed precipitate phases prevents stress concentration. The combined action of these factors increases the hardness of the welding joint.

3.4. Fracture characteristics

Fig. 15 is the force-displacement curve of the joint before and after adding the interlayer. The area under the force–displacement curve represents the energy absorbed before the welding joint fractures [39].

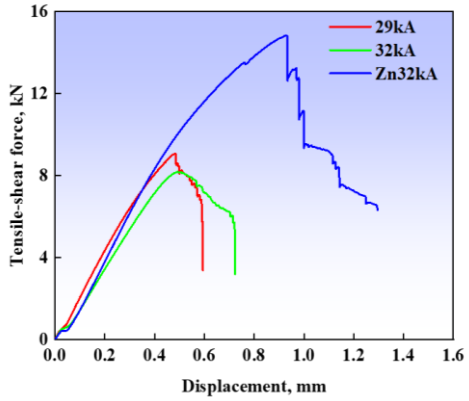


Fig. 15. Force–displacement curves of the welding joints before and after interlayer addition

Fig. 16 shows the toughness and the tensile shear force for the two types of welding. The toughness and tensile shear force of the welding joint are low in the absence of an interlayer. The toughness for the Zn-RSW joint is 11.28 J, which is 245 % greater than that without the interlayer (3.27 J).

4. CONCLUSIONS

In this study, RSW was carried out on a 3 mm thick 7075 aluminum alloy with a 50 μm thick Zn interlayer. The effects of adding the Zn interlayer on the macroscopic morphology, microstructure, precipitated phase, and mechanical properties of the RSW joint were systematically studied. The following conclusions were drawn.

1. The maximum tensile shear force sustained by a Zn-RSW joint is 14.29 kN, which is 51.5 % greater than that for a RSW joint (9.43 kN). The toughness work increases from a RSW joint is 3.27 J to a Zn-RSW joint is 11.28 J. The Zn-RSW joint is is 245 % higher than RSW joint.

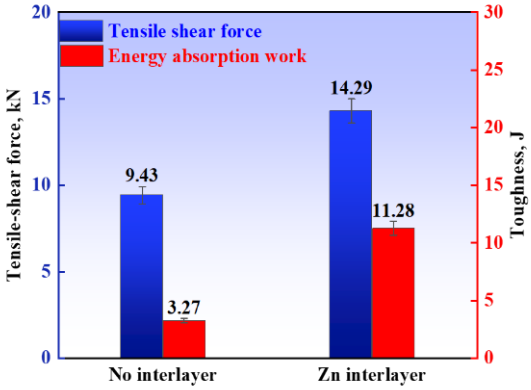


Fig. 16. Tensile shear force and toughness

2. The Zn-RSW joint has relatively high strength and toughness. The addition of a Zn interlayer to a RSW joint refines the grain size of the equiaxed grain zone from 32.9 μm to 25.4 μm (a 29.5 % decrease) and improves the joint microhardness.
3. Addition of the Zn interlayer considerably increases the number of T phases while making the phase distribution more uniform. The fine second phase particles can pin the grain boundary, effectively hinder the grain growth, and strengthen the joints through the second phase strengthening mechanism. The network-like or strip shape of the RSW joint is transformed into a point-like or short strip shape for the Zn-RSW joint, and the number of crack defects are also considerably reduced.
4. The added Zn interlayer fills the gap between the plates, increases the contact area between the plates, and reduces the contact resistance, thereby reducing the heat input to the weld heat and facilitating grain refinement.

Acknowledgments

The authors would like to acknowledge the financial support of the National Natural Science Foundation of China (Grant No. 51665044), the Natural Science Foundation of Inner Mongolia Autonomous Region (Grant Nos. 2021MS05009, 2021MS05021 and 2025MS05093), the Fundamental Research Funds for Universities Directly under the Inner Mongolia Autonomous Region (Grant No. JY20220229, No. JY20220252 and No. JY20220028) and Inner Mongolia Autonomous Region first-class discipline scientific research special project (Grant No. YLXKZX-NGD-002).

REFERENCES

1. **Jiang, D., Zhang, Q., Zhao, M., Xia, H., Wang, S., Li, Y.** Effects of Welds Distribution and High-low Temperature Humidity Alternating Aging on Sealing Performance of

Weld-bonded Stainless Steel Structures *Journal of Manufacturing Processes* 48 2019: pp. 77 – 85. https://doi.org/10.1016/j.jmapro.2019.10.017

2. **Cho, D., Ghassemi-Armaki, H., Stoughton, T.B., Carlson, B.E., Sung, H., Hwang, J., Legarth, B.N, Whan, J.** Fracture Mechanisms of Al-steel Resistance Spot Welds: The Role of Intermetallic Compound Phases *Engineering Fracture Mechanics* 311 2024: pp. 110520. https://doi.org/10.1016/j.engfracmech.2024.110520
3. **Ren, S.D., Huang, W.J., Ma, N.S., Watanabe, G, Zhang, Z.G., Deng, W.Z.** Numerical Modeling from Process to Residual Stress Induced in Resistance Spot Welding of DP980 Steel *The International Journal of Advanced Manufacturing Technology* 125 (7 – 8) 2023: pp. 3563 – 3576. https://doi.org/10.1007/s00170-023-10845-z
4. **Okada, T., Ueda, H., Miyazaki, Y., Yasuyama, M., Fujii, H.** Effect of Strength of Steel Sheets on Peel Tensile Strength and Failure Mode of Dissimilar Joint of Spot Welds *Welding International* 37 (5) 2023: pp. 295 – 308. https://doi.org/10.1080/09507116.2023.2202967
5. **Florea, R.S., Solanki, K.N., Bammann, D.J., Baird, J.C., Jordon, J.B., Castanier, M.P.** Resistance Spot Welding of 6061-T6 Aluminum: Failure Loads and Deformation *Materials & Design* 34 2012: pp. 624 – 630. https://doi.org/10.1016/j.matdes.2011.05.017
6. **Lu, K.Y., Qin, H.X., Bai, R.S., Du, H.J., Qi, J.S., Zhu, M.S., Shao, Y., Wang, D.W., Li, F.J.** Enhancing Aesthetics, Hardness and Corrosion Resistance of Aluminum Alloy Via Deposition of Al/Si/AlN Coatings *Journal of Alloys and Compounds* 1010 2025: pp. 176994. https://doi.org/10.1016/j.jallcom.2024.176994
7. **Ma, Y.X., Wang, P., Ji, W.A., Chen, R.** Effect of Adding $Sr(OH)_2$ on the Formation Process of 2024 Aluminum Alloy Micro-arc Oxidation Coatings *Materials Letters* 377 2024: pp. 137552. https://doi.org/10.1016/j.matlet.2024.137522
8. **Zhang, P., Zhang, S.T., Ge, S., Jiang, X.M., Chen, X.** Study on the Friction and Wear Properties of 7075-T6 Aluminum Alloy Enhanced by Milling and Ultrasonic Impact Treatment *Vacuum* 230 2024: pp. 113699. https://doi.org/10.1016/j.vacuum.2024.113699
9. **Fritsche, S., Schindler, F., de Carvalho, W.S., Amancio-Filho, S.T.** Wear Mechanisms and Failure Analysis of a Tool Used in Refill Friction Stir Spot Welding of AA6061-T6 *Wear* 560 2025: pp. 205610. https://doi.org/10.1016/j.wear.2024.205610
10. **Gogoi, S., Banerjee, S., Bhadra, R., Mondal, A.K., Roy, P.** Structure-Property Correlation for Friction Stir Welded Joints of 2219Al Alloys Micro-Alloyed with Cd *Materials Chemistry and Physics* 329 2025: pp.130051. https://doi.org/10.1016/j.matchemphys.2024.130051
11. **Das, S.** Life Cycle Energy and Environmental Assessment of Aluminum-intensive Vehicle Design *SAE International Journal of Materials and Manufacturing* 7 2014: pp. 588 – 595. https://doi.org/10.4271/2014-01-1004
12. **Luo, Z., Ao, S., Chao, Y.J.** Application of Pre-Heating to Improve the Consistency and Quality in AA5052 RSW *Journal of Materials Engineering and Performance* 24 (10) 2015: pp. 3881 – 3891. https://doi.org/10.1007/s11665-015-1704-x
13. **Guo, J., Bi, J., Wang, S., Li, Y., Manladan, S.M., Luo, Z.** Modeling the Effect of Electrode Morphology on Mg/Steel Resistance Spot Welding *International Journal of Materials and Manufacturing* 120 (1 – 2) 2022: pp. 137 – 148. https://doi.org/10.1007/s00170-021-08547-5
14. **Soomro, I.A., Pedapati, S.R.** Application of in Situ Post Weld Heat Treatment Using Double Pulse Technology and its Effect on Microstructure and Mechanical Performance of Resistance Spot Welded HSLA350 Steel *International Journal of Advanced Manufacturing Technology* 105 (7 – 8) 2019: pp. 3249 – 3260. https://doi.org/10.1007/s00170-019-04569-2
15. **Mazur, W., Kyriakopoulos, A., Bott, N., West, D.** Use of Modified Electrode Caps for Surface Quality Welds in Resistance Spot Welding *Journal of Manufacturing Processes* 22 2016: pp. 60 – 73. https://doi.org/10.1016/j.jmapro.2016.01.011
16. **Manladan, S.M., Yusof, F., Ramesh, S., Fadzil, M., Luo, Z., Ao, S.** A Review on Resistance Spot Welding of Aluminum Alloys *International Journal of Advanced Manufacturing Technology* 90 (1 – 4) 2017: pp. 605 – 634. https://doi.org/10.1007/s00170-016-9225-9
17. **Du, H.M., Bi, J., Zhang, Y., Wu, Y.D., Li, Y., Luo, Z.** The Role of the Partial Melting Zone in the Nugget Growth Process of Unequal-Thickness Dissimilar Aluminum Alloy 2219/5A06 Resistance Spot Welding *Journal of Manufacturing Processes* 45 2019: pp. 304 – 311. https://doi.org/10.1016/j.jmapro.2019.06.026
18. **Xia, Y.J., Su, Z.W., Li, Y.B., Zhou, L., Shen, Y.** Online Quantitative Evaluation of Expulsion in Resistance Spot Welding *Journal of Manufacturing Processes* 46 2019: pp. 34 – 43. https://doi.org/10.1016/j.jmapro.2019.08.004
19. **Meng, X.Y., Song, F., Lin, D.Y., Li, H.Y., Fu, C., Xia, H.B., Chen, X., Wu, L.J., Chen, B., Tan, C.W., Song, X.G.** Effect of the Thickness of Cu Interlayer on Dissimilar Laser Welding of 304 Stainless Steel to Tantalum *Optics and Laser Technology* 157 2023: pp. 108727. https://doi.org/10.1016/j.optlastec.2022.108727
20. **Chen, J.B., Yuan, X.J., Hu, Z., Li, T., Wu, K.L., Li, C.** Improvement of Resistance-Spot-Welded Joints for DP 600 Steel and A5052 Aluminum Alloy with Zn Slice Interlayer *Journal of Manufacturing Processes* 30 2017: pp. 396 – 405. https://doi.org/10.1016/j.jmapro.2017.10.009
21. **Lara, B., Giorjao, R., Ghassemi-Armaki, H., Ramirez, A.** Fe-Al Intermetallic Suppression of Dissimilar RSW Joints Using Stainless-Steel Interlayers *Science and Technology of Welded and Joining* 28 (6) 2023: pp. 461 – 467. https://doi.org/10.1080/13621718.2023.2176046
22. **Zhang, Y., Zhou, Z.Y., Fu, Y.Q., Li, H., Li, Z.X., Mariusz, B., Senkara, J.** Effects of Al/Zn Interlayer on the Solidification Path and Liquation Cracking Susceptibility of AZ31/ZK61 Dissimilar Magnesium Alloy Resistance Spot Welding Joints *Journal of Manufacturing Processes* 75 2022: pp. 60 – 71. https://doi.org/1016/j.jmapro.2021.12.017
23. **Liu, C., Zhang, J., Shi, H., Li, Q.** Influence of Interlayer Nb on the Performance of Joint Between Titanium and Steel Welded by Resistance Spot Welding *Journal of Materials Engineering and Performance* 31 (2) 2022: pp. 1155 – 1162. https://doi.org/10.1007/s11665-021-06229-7
24. **Qin, Q., Zhao, H., Zhang, Y., Li, Y., Wang, Z.** Microstructures and Mechanical Properties of Al-Mg_2Si-Si Alloys Resistance Spot Welded with Al-Si Interlayers

Journal of Materials Research and Technology 8 (5) 2019: pp. 4318 – 4332. https://doi.org/10.1016/j.jmrt.2019.07.043

25. **AWS D8.2M:2017.** Specification for Automotive Weld Quality-Resistance Spot Welding of Aluminum *American Welded Societym*, 2017. https://webstore.ansi.org/standards/aws/awsd82m2017
26. **Rajak, B., Kishore, K., Mishra, V.** Investigation of a Novel TIG-Spot Welding Vis-à-Vis Resistance Spot Welding of Dual-Phase 590 (DP590) Steel: Processing-Microstructure-Mechanical Properties Correlation *Materials Chemistry and Physics* 296 2023: pp. 127254. https://doi.org/10.1016/j.matchemphys.2022.127254
27. **Meng, X., Zhang, D., Zhang, W., Qiu, C., Liang, G., Chen, J.** Microstructure and Mechanical Properties of a High-Zn Aluminum Alloy Prepared by Melt Spinning and Extrusion *Journal of Alloys and Compounds* 819 2020: pp. 152990. https://doi.org/10.1016/j.jallcom.2019.152990
28. **Sivasankaran, S., Ramkumar, K.R., Ammar, H.R., Al-Mufadi, F.A., Alaboodi, A.S., Irfan, O.M.** Microstructural Evolutions and Enhanced Mechanical Performance of Novel Al-Zn Die-Casting Alloys Processed by Squeezing and Hot Extrusion *Journal of Materials Processing Technology* 292 2021: pp. 117063. https://doi.org/10.1016/j.jmatprotec.2021.117063
29. **Choi, I., Kim, Y., Ahn, B., Kawasaki, M., Langdon, G.T., Jang, J.** Evolution of Plasticity, Strain-Rate Sensitivity and the Underlying Deformation Mechanism in Zn–22% Al During High-Pressure Torsion *Scripta Materialia* 75 (15) 2014: pp. 102 – 105. https://doi.org/10.1016/j.scriptamat.2013.12.003
30. **Figueiredo, B.R., Kawasaki, M., Langdon, G.T.** The Role of Grain Size in Achieving Excellent Properties in Structural Materials *Journal of Materials Research and Technology* 30 2024: pp. 3448 – 3462. https://doi.org/10.1016/j.jmrt.2024.04.059
31. **Li, J.Q., Li, X.H., Xu, T.Y., Yan, H., Mao, Y.Z., Chen, R.S.** Regulating the Grain Refinement and Rolling Properties of Coarse-Crystalline Mg-Zn-Gd-Ca-Mn Alloy Through Multi-Pass Cold Rolling and Annealing *Materials Science and Engineering: A* 911 2022: pp. 146940. https://doi.org/10.1016/j.msea.2024.146940
32. **Zhang, Z.J., Yuan, L., Ma, J.P., Zheng, M.Y., Shan, D.B., Guo, B.** Role of <a> and <c+a> Dislocations on the Room-Temperature Grain Boundary Migration in a Deformed Mg Alloy *International Journal of Plasticity* 172 2024: pp. 103862. https://doi.org/10.1016/j.ijplas.2023.103862
33. **Liu, J., Zhu, G., Mao, W., Subramanian, S.V.** Modeling of Critical Grain Size for Shifting Plasticity Enhancement to Decrease by Refining Grain Size *Materials Science and Engineering: A* 607 (23) 2014: pp. 302 – 306. https://doi.org/10.1016/j.msea.2014.04.012
34. **Xiao, L., Liu, L., Esmaeili, S., Zhou, Y.** Microstructure Refinement After the Addition of Titanium Particles in AZ31 Magnesium Alloy Resistance Spot Welds *Metallurgical and Materials Transactions* 43A (2) 2012: pp. 598 – 609. https://doi.org/10.1007/s11661-011-0881-y
35. **Li, R.X., Qin, X.Z., Zhao, J.L., Li, B., Zhao, W., Zhou, Y., Li, B.K., Zhang, J.L.** Effect of Zn on Microstructure and Properties of Al-4.5 % Mg-1.0 % Mn-0.1 % Zr Alloy *Heat Treatment of Metals* 50 (09) 2025: pp. 278 – 286. https://link.cnki.net/doi/10.13251/j.issn.0254-6051.2025.09.044
36. **Soomro, I.A., Pedapati, S.R., Awang, M., Alam, M.A.** Effects of Double Pulse Welding on Microstructure, Texture, and Fatigue Behavior of DP590 Steel Resistance Spot Weld *The International Journal of Advanced Manufacturing Technology* 125 (3) 2023: pp. 1271 – 1287. https://doi.org/10.1007/s00170-022-10704-3
37. **Ren, B.K., Zhou, K., Yao, P., Wang, G., Yu, W.X.** Sonotrode Design and Spatial-Temporal Configuration Strategy of Ultrasonic Vibration for Aluminum/Steel Resistance Spot Welding *The Journal of Materials Processing Technology* 341 2025: pp. 118897. https://doi.org/10.1016/j.jmatprotec.2025.118897
38. **Liu Z.Y., Chao B.X., Li Z.Y.** Optimization of Resistance Spot Welding Process and Study on Mechanical Properties of Joints of Copper/Aluminum Dissimilar Alloy with Copper Plate Spacer *Welding Technology* 4 2025: pp. 77 – 83. http://dianda.cqvip.com/Qikan/Article/Detail?id=7200843496
39. **Deng, W., Li, D., Sang, Y., Cao, Z., Li, Y.** Microstructure and Mechanical Properties of WRe/GH3128 Alloy Electron Beam Welded Joint *Materials Science and Engineering A-Structural Materials Properties Microstructure and Processing* 882 2023: pp. 145400. https://doi.org/10.1016/j.msea.2023.145400

© Li et al. *2026* Open Access This article is distributed under the terms of the Creative Commons Attribution 4.0 International License (http://creativecommons.org/licenses/by/4.0/), which permits unrestricted use, distribution, and reproduction in any medium, provided you give appropriate credit to the original author(s) and the source, provide a link to the Creative Commons license, and indicate if changes were made.